Highly Sensitive Analysis of Boron and Lithium in Aqueous Solution Using Dual-Pulse Laser-Induced Breakdown Spectroscopy

ARTICLE *in* ANALYTICAL CHEMISTRY · NOVEMBER 2011

Impact Factor: 5.64 · DOI: 10.1021/ac2021689 · Source: PubMed

analytical chemistry

ARTICLE

pubs.acs.org/ac

Highly Sensitive Analysis of Boron and Lithium in Aqueous Solution Using Dual-Pulse Laser-Induced Breakdown Spectroscopy

Dong-Hyoung Lee, Sol-Chan Han, Tae-Hyeong Kim, and Jong-Il Yun*

Department of Nuclear and Quantum Engineering, KAIST 219 Daehak-ro, Yuseong-gu, Daejeon 305-701, Republic of Korea

ABSTRACT: We have applied a dual-pulse laser-induced breakdown spectroscopy (DP-LIBS) to sensitively detect concentrations of boron and lithium in aqueous solution. Sequential laser pulses from two separate Q-switched Nd:YAG lasers at 532 nm wavelength have been employed to generate laser-induced plasma on a water jet. For achieving sensitive elemental detection, the optimal timing between two laser pulses was investigated. The optimum time delay between two laser pulses for the B atomic emission lines was found to be less than 3 μs and approximately 10 μs for the Li atomic emission line. Under these optimized conditions, the detection limit was attained in the range of 0.8 ppm for boron and 0.8 ppb for lithium. In particular, the sensitivity for detecting boron by excitation of laminar liquid jet was found to be excellent by nearly 2 orders of magnitude compared with 80 ppm reported in the literature. These sensitivities of laser-induced breakdown spectroscopy are very practical for the *online* elemental analysis of boric acid and lithium hydroxide serving as neutron absorber and pH controller in the primary coolant water of pressurized water reactors, respectively.

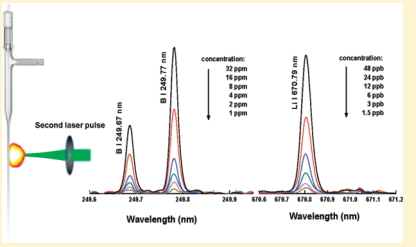

In pressurized water reactors (PWRs), water chemistry conditions—including pH, electrochemical potential (ECP), and concentration of dissolved metal ions—have a significant impact on corrosion behaviors of structural materials and fuel cladding, fuel performance, and radiation management. pH control of the primary reactor coolant water containing boric acid (H_3BO_3, 900−1800 ppm at the beginning of cycle, BOC), as a neutron absorber (called a "chemical shim") is conducted by adding isotopically pure lithium hydroxide (^{7}LiOH, 2−5 ppm lithium at BOC).[1] The pH strategy of the primary coolant water is set to reduce crud deposition on fuel rods and to minimize radiation fields. The value of pH at the working temperature should be controlled above 6.9 to prevent the corrosion of structural materials by maintaining the proper level of LiOH concentration during one fuel cycle. The concentration of boron in reactor coolant water is decreased progressively with increasing burnup, and the lithium concentration is gradually increased because of the nuclear reaction of ^{10}B(n,α)^{7}Li. However, increasing the lithium level may be a risk regarding corrosion resistance of zirconium alloy as a fuel cladding material, so it is important to monitor the concentration of boric acid and lithium hydroxide regularly.

For routine monitoring of coolant water quality in PWRs, several analytical methods (such as gravimetric analysis, volumetric analysis, spectrometry, and neutron activation analysis) have been utilized. At present, the boron concentration has been determined either via an in situ measurement technique using absorption of moderated neutrons without sample preparation, or by titration as an off-line method.[2] For the determination of the lithium concentration, atomic absorption spectrometry[3] and inductively coupled plasma atomic emission spectroscopy[4] have been widely used. In the case of most analytical techniques, with the exception of neutron absorption, however, samples should be taken from sampling lines after a cooling process and delivered to the off-line instruments. During this procedure, the samples should be handled carefully to avoid additional exposure to radiation. Therefore, it is necessary to develop a rapid qualitative and quantitative analytical technique, which can simultaneously detect boron and lithium ion concentration without any risk of radiation exposure during and after sampling and the analysis procedure.

Here, we have introduced laser-induced breakdown spectroscopy (LIBS), which employs two sequential laser pulses to determine boron and lithium concentrations in water. The LIBS has been used in a variety of research fields as an analytical technique for solid samples,[5−7] ions and colloids in solution,[8−11] and gases.[12] However, this technique has crucial limitations, because of its lower sensitivity, when compared to other spectrometric methods. One promising method to improve LIBS sensitivity is the use of a dual-pulse configuration. Cremers et al.[13] demonstrated the 15-fold-higher detection sensitivity for boron in water by LIBS with a dual-pulse approach than with a single-pulse approach. Besides, Nakamura et al.[14] reported that the detection limit of colloidal and particulate iron in water decreases from 600 ppb by single-pulse excitation to 16 ppb by dual-pulse excitation. These enhancement effects have been explained by several mechanisms, such as reheating by the second laser,[15] a larger plasma volume,[16] increased ablated mass and higher plasma temperature,[17] rarified atmosphere[18] and so on. Until now, the analysis of lithium in solution was reported in numerous articles,[9,11,13,19] whereas a few studies were reported

Received: August 16, 2011
Accepted: November 4, 2011
Published: November 04, 2011

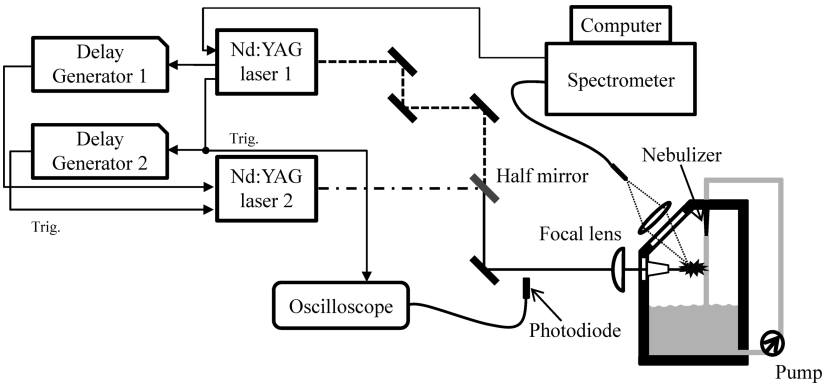

Figure 1. Schematic drawings of the experimental setup for dual-pulse laser-induce breakdown spectroscopy.

on the applications of LIBS to the monitoring of boron in liquid.[13,20]

In this paper, we have reported the limit of detection for boron and lithium in water using DP-LIBS. The laser-induced plasma was created at the surface of laminar liquid jet in the closed system, which is applicable to hazardous or radioactive aqueous solutions. The optimal interpulse delay time between two laser pulses was investigated to achieve sensitive elemental detection. The lifetimes of each element were measured to characterize the temporal plasma emission behavior. Hydrogen (H_β) and Eu emission lines were utilized for the determination of electron number density and plasma temperature, respectively. This study showed that DP-LIBS provides the *online* capability to measure boron and lithium metal ions in liquid with very high sensitivity.

EXPERIMENTAL SECTION

Apparatus. The sequential pulses were produced by two Q-switched Nd:YAG lasers (Continuum Co., Surelite-20, wavelength = 532 nm, pulse width = 6 ns, repetition rate = 20 Hz). The first laser was computer-controlled and the laser energy and interpulse delay of the second laser were controlled by two delay generators (Stanford Instruments, Model DG535), which were triggered by the first laser, as shown in Figure 1. The time difference between two laser pulses was continuously monitored by a rapid photodiode (Newport, Model 818-BB-21) coupled with an oscilloscope (Tektronix, Model TDS 380P). The optical beam geometry was a collinear configuration, i.e., both pulses propagate in the same direction and are delivered perpendicular to the sample surface. The laser pulses were focused onto the surface of a water jet using a fused-silica plano-convex lens with a focal length of 56.0 mm and the lens-to-sample distance was optimized to achieve the highest emission intensity of B doublet at 249.67 and 249.77 nm. The pulse energies used for the first and second lasers were 30 mJ and 100 mJ, respectively. All experiments were performed in a closed aerobic liquid jet system under atmospheric pressure.

A laminar liquid jet was formed by a nebulizer (Glass Expansion, Model AR35-1-FS6E) with a peristaltic pump, creating a 0.42 mm stable jet in size at liquid flow rate of 41.5 mL/min. The laser was focused ~10 mm below the jet exit, where the liquid flow is laminar. The homemade sample cell with a closed circulation loop system was made of polyethylene. To avoid contamination of the focal lens from ejected and scattered droplets caused by laser-induced shock wave, a block with a small hole was placed between focal lens and water jet. A quartz window was set at an angle of 45°, relative to the laser beam direction for plasma emission detection, as illustrated in Figure 1.

Table 1. Spectral Lines Used for the LIBS Intensities[a]

Spectral Lines (nm)			
B(I)	Li(I)	Eu(I)	Eu(II)
249.67 (4.964)	670.79 (1.848)	459.40 (2.698)	372.49 (3.328)
249.77 (4.964)		462.72 (2.679)	381.96 (3.245)
		466.18 (2.659)	390.71 (3.379)
			393.04 (3.361)
			397.19 (3.328)
			412.97 (3.001)
			420.50 (2.948)
			443.55 (3.001)

[a] The upper excitation level (in eV) is given in parentheses.

For the purpose of multielemental analysis, an echelle spectrometer (LLA, Model ESA3000) providing wide wavelength range (200−780 nm) and high spectral resolution ($\lambda/\Delta\lambda$ = 40 000) was utilized. The plasma emission was collimated and focused by a 30-mm fused-silica focal lens onto the entrance of fiber optic with a core diameter of 1.0 mm and delivered to the spectrometer. The delivered plasma emission light was dispersed by an echelle grating and a prism to generate a two-dimensional spectral image and converted to the electrical signal with intensified charge-coupled device (ICCD). The detector gate delay was adjusted with respect to the second laser pulse.

Chemicals. Solutions were prepared with the use of boric acid (Junsei Chemical Co., 99.5% purity), lithium hydroxide monohydrate (Junsei Chemical Co., ≥98% purity), and europium chloride (Aldrich, 99.99% purity). Deionized water (Millipore, Milli-Q Synthesis) was used for the preparation of desired metal ion concentrations in the present work.

RESULTS AND DISCUSSION

Effect of Interpulse Delay Time. It is well-known that the time delay between two laser pulses plays an important role in the enhancement of emission signals, because of the coupling of the second laser with the plasma generated by the first laser pulse and sample surface.[15,21−23] For this reason, we simultaneously observed the emission signal intensities of atomic and ionic lines of boron (30 ppm), lithium (20 ppb), and europium (10 ppm) by varying the interpulse delay time from 1 μs to 25 μs. In this

dx.doi.org/10.1021/ac2021689 |*Anal. Chem.* 2011, 83, 9456–9461

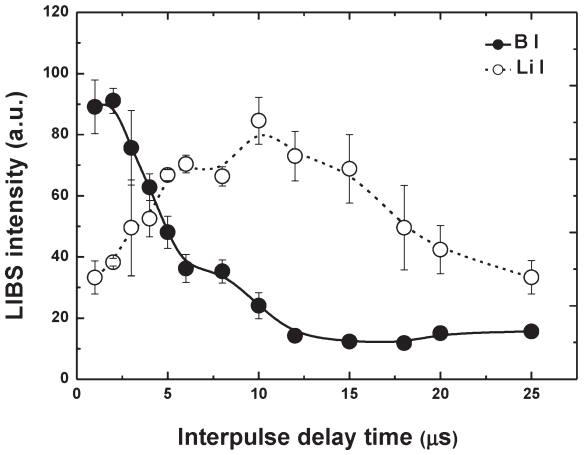

Figure 2. Dependence of LIBS intensities of B(I) and Li(I) on interpulse delay time, using 30 ppm boron and 20 ppb lithium solutions.

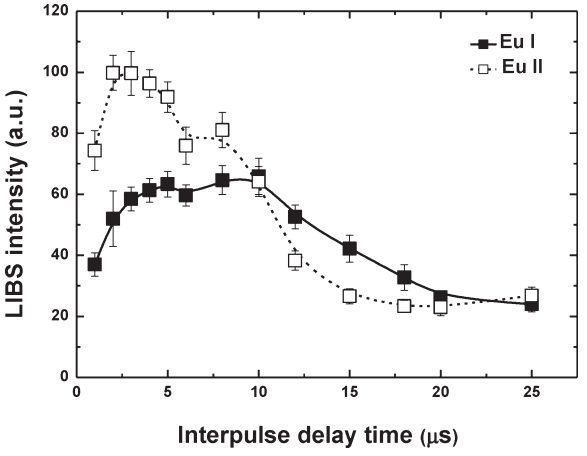

Figure 3. Dependence of Eu(I) and Eu(II) emission intensities on interpulse delay time at the solution concentration of 10 ppm Eu.

experiment, the detector gate delay time was kept at 5 μs, relative to the second laser pulse, and the detector gate width was fixed at 40 μs. For low uncertainty and high reproducibility, LIBS intensities were obtained with the sum of intensities for all the emission lines listed in Table 1.

Figure 2 shows the influence of interpulse delay on the emission intensities of B(I) at 249.67 and 249.77 nm and Li(I) at 670.79 nm. While the emission intensity for B atomic lines suddenly dropped off after a 2-μs delay, the signal for the Li atomic line reached a maximum at a 10-μs delay and decreased for higher interpulse intervals. For metal samples,[18,23] the optimal interpulse delay for higher excitation energy levels of the emission lines was determined at a longer value than for a lower one. In contrast, the excitation energy level for lithium is lower than that for boron, as shown in Table 1, while the optimal delay time between two laser pulses for lithium was found to be a longer value in this work.

To identify further relationships between the optimal delay time and the excitation energy level in a liquid jet system, the variation of atomic and ionic emission lines for Eu were taken into account, as shown in Figure 3. The strong emission lines of Eu(II) at 381.96, 393.04, 412.97, and 420.50 nm were excluded in this experiment, because these four peaks were saturated for a

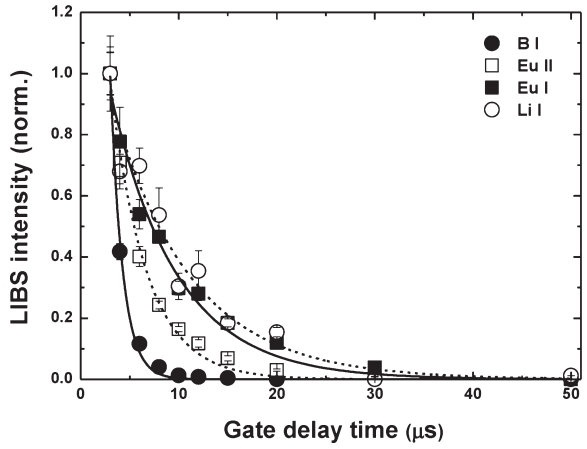

Figure 4. Time evolution of emission intensities for B(I), Li(I), Eu(I), and Eu(II) emission lines by dual-pulse excitation of 20 ppm boron, 20 ppb lithium, and 4 ppm europium solutions.

shorter interpulse delay time. The atomic emission lines of Eu had lower intensities than the ionic emission lines for shorter interpulse delay. However, emission intensities of the atomic lines exceeded those for the ionic emission lines as the interpulse delay time increased beyond 10 μs. The ionic emission lines reached a maximum intensity at ~2−5 μs delay and then started to decrease, but the atomic emission lines showed a somewhat flat profile in the delay time range of 3−10 μs.

Similar results were reported by Rai et al.[24] They observed that the atomic line emission of Mg shows a broader profile with interpulse delay than its ionic line emission. Moreover, the optimum interpulse delays for neutral atoms and ions of Mg such as Mg(I) at 285 nm and Mg(II) at 279 and 280 nm were roughly in the same time range of 2−3 μs. The plateau-like behavior of the atomic emission of Li and Eu indicated that these neutral atoms could be sustained longer at any place in the expanding plasma plume, whereas ions of Eu were not able to endure for a longer time in the plasma plume during its expansion.[24] The decreasing behavior of emission intensity could be explained by the difference of interactions between the second laser pulse and the plasma generated by the first laser pulse with increasing time interval of two laser pulses. As the hot plasma was continuously cooled by the process of atomization, the density of ions and atoms in plasma plume would decrease, and the absorbing efficiency of the plasma for the second laser could be significantly affected.

It is noteworthy that the atomic emission of B underwent the most rapid decrease in signal intensity, compared to other elements. The rapid decease of B atomic emission intensity was not affected by the weight of element, because Li is lighter than B. The optimum delay time and intensity behavior of each element with increasing interpulse delay should be explained in terms of the temporal evolution of each species and the plasma temperature.

Time Dependency of the Emission Line. An atomic lifetime is defined as the inverse of the sum of the rates of all spontaneous transitions (A_{ki}, transition probability, Einstein A coefficient) from a higher energy level to a lower one.[25] Under atmospheric pressure, the temporal behavior of emission does not follow the theoretical lifetime, because of the disturbance of relaxation of excited species by collisions, quenching, and energy transport phenomena.[9] The plasma produced by dual-pulse lasers cools

slowly and the excitation is sustained for a longer time, compared to the plasma generated by a single-pulse laser, because of the reduction of air pressure and the confinement of plasma by shockwave front created by the first laser pulse.[26,27] For this reason, a significant enhancement in emission intensity can be achieved.

Results of the dual-pulse excitation are shown in Figure 4 for increasing gate delay times, where interpulse delay time was kept at 5 μs. The gate delay was changed from 3 μs to 50 μs, with respect to the second laser pulse, because the emission intensities of the N(I) and O(I) triplet (777.19, 777.41, and 777.53 nm) were too strong at a gate delay time of 1−2 μs. In this time range, all emission lines from each species showed a similar decrease in intensity, and a monoexponential temporal behavior was observed. Using these data, the lifetime of each species was calculated by an exponential curve fitting algorithm. The lifetimes (τ) of B(I), Eu(II), Eu(I), and Li(I) emission lines were determined to be 1.05 ± 0.05, 3.38 ± 0.19, 6.12 ± 0.63, and 8.09 ± 1.63 μs, respectively. The lifetime of Li(I) at 670.79 nm was greater by a factor of ~50, compared to that measured with single-pulse LIBS in the bulk solution (Li(I) at 670.79 nm: τ = 151 ± 17 ns).[9]

For dual-pulse excitation system, there are two plausible processes occurring in the plasma plume: (1) absorption of the second laser pulse in the plume of the plasma initiated by the first laser pulse and (2) new plasma formation by the remaining second laser pulse.[27,28] Considering the processes, when the species cannot be present for a longer time in the plume, the first process will be less effective to the enhancement of signal intensity. In our configuration, the lifetime of B atomic emissions at 249.67 and 249.77 nm was the shortest, and the optimal interpulse delay time for B was obtained at earlier time delay, compared to other species. In contrast, the Li atomic emission line at 670.79 nm could be sustained for a relatively long time in the plasma and the optimum delay time for the Li neutral atom was measured at a longer time delay than that for the neutral B atom. It was shown that the longer the lifetime of the elements is, the larger the optimum interpulse delay becomes. Furthermore, it was found that the lifetime of atomic emission lines has a correlation with the first ionization energy for each element. The ionization energies of B, Eu, and Li are 8.298, 5.670, and 5.392 eV, respectively. It represents that the element B is relatively difficult to be ionized by multiphoton ionization (2.331 eV for a 532-nm laser wavelength), compared to Eu and Li. The number of excited atomic species can be partially attributed by the electron-ion recombination (free-bound transitions) in the plasma. This partial contribution to the increased atomic species population at excited states may result in the prolonged lifetime of atomic emission for elements with lower ionization energy in a relative manner. A comparable correlation between the lifetime and the ionization energy could be deduced based on literature data as well.[9]

Electron Density and Plasma Temperature. The laser-induced plasma is characterized by parameters such as electron density and plasma temperature. The electron density is commonly determined using spectroscopic techniques, such as Stark broadening, Saha−Eggert ionization equilibrium, absolute continuum intensity, etc.[29,30] In this study, the electron density was determined in terms of the Stark broadening of hydrogen Balmer line (H_β: 486.13 nm). The theoretical electron contribution to the full width at half-maximum (fwhm), $\Delta\lambda^S_{1/2}$ of H or H-like ions is related to the electron density N_e by the following expression:[31,32]

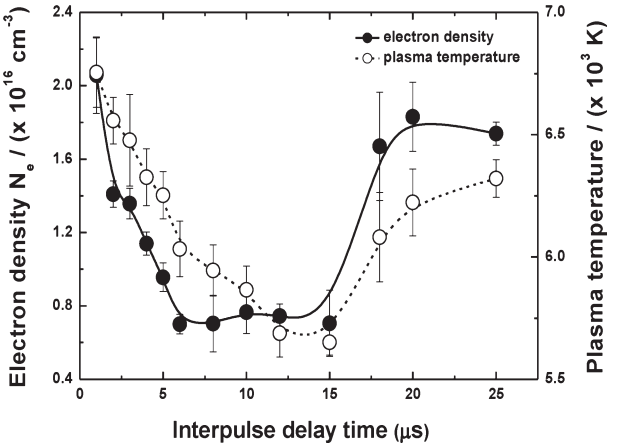

Figure 5. Dependence of electron density and plasma temperature on interpulse delay time.

$$\Delta\lambda^S_{1/2} = 2.5 \times 10^{-9}\alpha_{1/2}N_e^{2/3} \quad (1)$$

where $\alpha_{1/2}$ is the fractional width at half-height of the Stark profile (expressed in angstroms per cgs field strength unit and tabulated in the literature[31]). When the electron density N_e is ~10^{16} cm^{-3} and the electron temperature is ~5 × 10^3 K, the fractional width $\alpha_{1/2}$ is 0.0808 Å. The ICCD gate delay time was 5 μs from the second laser pulse. The fwhm of H_β was obtained after correcting the measured line width for the instrumental and Doppler broadening contributions.

Plasma temperature is often determined using the relationships between transition line intensities from (a) the same ionization stage (Boltzmann plot) and (b) the subsequent ionization stages of the same element (Saha equation).[33] In this study, the plasma temperature was calculated by Saha−Boltzmann analysis, which can provide better accuracy, because of a large difference of the upper-state energy of the two lines. The formula is as follows:

$$\frac{I_{ion}}{I_{atom}} = \left(\frac{gA}{\lambda}\right)_{ion}\left(\frac{\lambda}{gA}\right)_{atom}\frac{2(2\pi m_e k)^{3/2}}{\hbar^3}\left(\frac{1}{N_e}\right)T^{3/2} \times \exp\left(-\frac{E_{ion} - E_{atom} + E_{IP} - \Delta E}{kT}\right) \quad (2)$$

where I is the line emission intensity, g the statistical weight of the upper level of the transition, A the transition probability, λ the transition wavelength, m_e the rest mass of electron, k the Boltzmann constant, $\hbar$ Planck's constant, N_e the electron density obtained by eq 1, T the temperature, $E_{ion,atom}$ the energies of the upper states of ion and atom, E_{IP} the ionization potential of the atom, and ΔE a correction to the ionization potential for interactions in the plasma.[33] A more-detailed description of the Saha−Boltzmann analysis is given in the literature.[34]

The ionic (390.71 and 397.19 nm) and atomic (459.40, 462.72, and 466.18 nm) emission lines of Eu were used to calculate the plasma temperature. The obtained electron density, plotted as a function of interpulse delay time, is shown in Figure 5, in addition to the plasma temperature. Before an interpulse delay time of 15 μs, the electron density and plasma temperature showed decreasing tendency and then changed suddenly after

dx.doi.org/10.1021/ac2021689 |Anal. Chem. 2011, 83, 9456–9461

Table 2. Detection Limits for Boron, Lithium, and Europium in Aqueous Solution with Different Interpulse Delays and Detector Gate Delays

interpulse delay (μs)	detector gate delay (μs)	B(I) (ppm)	Li(I) (ppb)	Eu(I) (ppm)	Eu(II) (ppm)
3	3.25	**0.8**[a]	28.7[a]	2.85[a]	0.86[a]
5	7	2.09[a]	1.70[a]	**0.43**[a]	**0.17**[a]
8	6	3.08[a]	1.2[a]	**0.45**[a]	**0.17**[a]
12	9		**0.8**[a]	0.47[a]	0.28[a]
		80[b], 1200[c]	6[c], 13[d]	0.03[e], 5.0[f]	

[a] This work (determination of LOD for S/N = 3σ). [b] Data in ref 13 for S/N = 2σ by dual pulse in bulk solution. [c] Data in ref 13 for S/N = 2σ by single pulse in bulk solution. [d] Data in ref 9 for S/N = 3σ by single pulse in bulk solution. [e] Data in ref 10 for S/N = 3σ by single pulse using Eu_2O_3 particles in bulk solution. [f] Data in ref. 10 for S/N = 3σ by single pulse using Eu^{3+} ions in bulk solution.

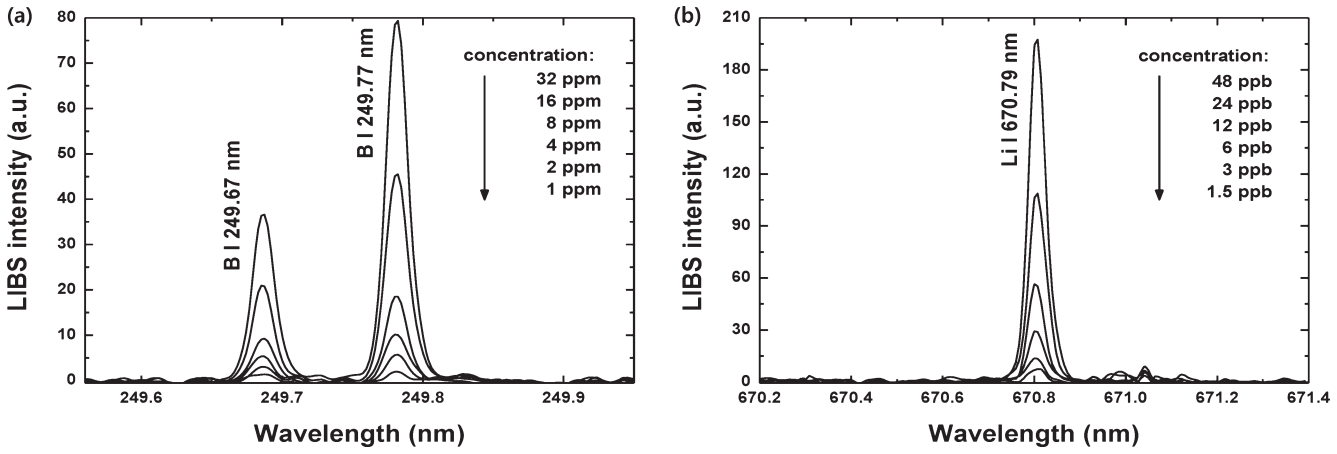

Figure 6. (a) Emission spectra of B(I) at interpulse delay of 3 μs and detector gate delay of 3.25 μs and (b) Li(I) at interpulse delay of 12 μs and detector gate delay of 9 μs.

15 μs. The initial decrease of number density and temperature could be caused by less absorption of the second laser pulse in the expanding plasma produced by the first laser pulse. After a time difference of 15 μs between two laser pulses, the first generated plasma rarely absorbed the next incoming laser pulse and the second laser pulse interacted with the surface of the water jet. By comparison with the results of interpulse delay dependence of analyte signals, it is of interest that only the B atomic emissions showed similar tendency with electron density and plasma temperature. Kumar et al. observed that the increasing interpulse delay time reduces the electron density, in agreement with the pattern of Mg(II) emission intensity at 279.5 nm.[35] However, at larger laser delay times, the observed electron density remained almost constant, and it was suggested that the signals are basically associated with the plasma produced by the second laser. Such dissimilar behaviors of electron density and plasma temperature at larger interpulse delay time comparing with the present results may be elucidated by different focal characteristics of the second laser such as focal position, focal length, and irradiance of the focused laser beam at the surface of the water jet. Mao et al. observed the behavior of the Si(I) emission intensity at 288.16 nm with increasing interpulse delay time, showing a similar tendency with plasma temperature.[17] Different behaviors of elements and species should be explained by considering several characteristics such as ionization energy of element, excitation level of emission lines, decay time of species in plasma plume, and matrix effect. Therefore, further investigations are necessary to prove the relationship between interpulse delay and line emission enhancement.

Limit of Detection. The limit of detection (LOD) for boron, lithium, and europium in aqueous solution was determined using DP-LIBS. After investigating the effects of interpulse delay and detector gate delay on the emission intensities of each species, four different experimental conditions were selected, as listed in Table 2. For the experiments, 1000 incident laser pulses were accumulated to obtain reasonable signal-to-noise ratio by averaging a set of five replicate measurements. Particularly, in the case of boron, interpulse delay, detector gate delay, and the gain value of spectrometer were cautiously controlled to be prevented from the oversaturation of the ICCD camera with 500 incident laser pulses. In the present work, the concentration calibration was carried out using all emission lines listed in Table 1. A series of emission spectra with varying the concentrations of boron and lithium are presented in Figure 6.

A plot of the measured emission intensity versus the sample concentration showed a simple linear relationship with good correlation. The detection limit (C_L) is given by

$$C_L = \frac{3\sigma}{S}$$

where S is the slope of a linear calibration relation and σ is the noise signal (standard deviation acquired from pure Milli-Q water). A comparison of the LOD values in the present work and those reported in the literature is presented in Table 2. As mentioned above, the experiments for detecting boron were found very sparsely in the literature, but only Cremers et al.[13] performed directly in liquid solution using single-pulse and

dual-pulse excitation. In the present work, the higher sensitivity for the boron measurement—2 orders of magnitude higher than that observed in the previous work,[13] was achieved using collinear and jet configuration for DP-LIBS. As expected, the LOD values were strongly dependent on the experimental parameters, such as interpulse delay and detector gate delay. It is of note that the Eu ionic emission was hardly detectable in bulk solution.[10] However, the intensities of Eu ionic emission lines were much stronger than its atomic emission lines in the present DP-LIBS configuration. It indicated that the present DP-LIBS system allows a much longer lifetime of plasma emission and higher plasma temperature.

Based on these results, DP-LIBS has been successfully demonstrated the applicability to the *online* analysis of boron and lithium in the primary coolant water of nuclear power plant, not only due to its rapid assay and ability for noncontact mode measurement, but also due to its superb sensitivity, even below the ordinarily operating concentrations of boron and lithium in primary reactor coolant water.

CONCLUSION

The dual-pulse laser-induced breakdown spectroscopy (DP-LIBS) has been successfully employed to sensitively detect boron and lithium metal ions in water, which are present for the chemistry control of the primary coolant water in pressurized water reactors (PWRs). To improve the detection sensitivity, the effect of interpulse delay on the emission signal intensity for each analyte was investigated in the closed laminar liquid jet system. The results evidenced very different behaviors of B and Li atomic emission intensities versus interpulse delay time. It was recognizable that the Li neutral species could be sustained for a longer time than the B atomic species in plasma plume by measuring lifetimes of B and Li emission lines. Characteristics of the plasma such as electron density and plasma temperature were analyzed with increasing interpulse delay time using H_β lines and Eu atomic and ionic emission lines. Under the optimized conditions, the detection limit of boron and lithium in water was achieved in the range of 0.8 ppm and 0.8 ppb, respectively. The DP-LIBS provides the possibility of *online* quality monitoring for the primary coolant water in nuclear power plants with a rapid and multielemental analytical approach.

AUTHOR INFORMATION

Corresponding Author

*Tel.: +82-42-350-3825. Fax: +82-42-350-3810. E-mail: jiyun@kaist.ac.kr.

ACKNOWLEDGMENT

This work was supported by the Nuclear R&D program through the National Research Foundation of Korea funded by the Ministry of Education, Science and Technology.

REFERENCES

(1) Lundgren, K.; Riess, R.; Strasser, A.; Sandklef, S. *LCC-1 (LWR Chemistry and Component Integrity Program) Annual Report*, ANT International, Sweden, 2005.

(2) International Atomic Energy Agency (IAEA). *High temperature on-line monitoring of water chemistry and corrosion control in water cooled power reactors*; IAEA-TECDOC-1303, 2002.

(3) Pybus, J.; Bowers, G. N., Jr. *Clin. Chem.* **1970**, *16*, 139–143.

(4) Fassel, V. A. *Science* **1978**, 183–191.

(5) Kagawa, K.; Hattori, H.; Ishikane, M.; Ueda, M.; Kurniawan, H. *Anal. Chim. Acta* **1995**, *299*, 393–399.

(6) Aragón, C.; Peñalba, F.; Aguilera, J. A. *Anal. Bioanal. Chem.* **2006**, *385*, 295–302.

(7) Corsi, M.; Cristoforetti, G.; Hidalgo, M.; Iriarte, D.; Legnaioli, S.; Palleschi, V.; Salvetti, A.; Tognoni, E. *Appl. Spectrosc.* **2003**, *57*, 715–721.

(8) Fichet, P.; Mauchien, P.; Wagner, J.-F.; Moulin, C. *Anal. Chim. Acta* **2001**, *429*, 269–278.

(9) Knopp, R.; Scherbaum, F. J.; Kim, J. I. *Fresenius, J. Anal. Chem.* **1996**, *355*, 16–20.

(10) Yun, J.-I.; Bundschuh, T.; Neck, V.; Kim, J.-I. *Appl. Spectrosc.* **2001**, *55*, 273–278.

(11) Samek, O.; Beddows, D. C. S.; Kaiser, J.; Kukhlevsky, S. V.; Liška, M.; Telle, H. H.; Young, J. *Opt. Eng.* **2000**, *39*, 2248–2262.

(12) Hohreiter, V.; Hahn, D. W. *Anal. Chem.* **2005**, *77*, 1118–1124.

(13) Cremers, D. A.; Radziemski, L. J.; Loree, T. R. *Appl. Spectrosc.* **1984**, *38*, 721–729.

(14) Nakamura, S.; Ito, Y.; Sone, K. *Anal. Chem.* **1996**, *68*, 2981–2986.

(15) Uebbing, J.; Brust, J.; Sdorra, W.; Leis, F.; Niemax, K. *Appl. Spectrosc.* **1991**, *45*, 1419–1423.

(16) Angel, S. M.; Stratis, D. N.; Eland, K. I.; Lai, T.; Berg, M. A.; Gold, D. M. *Fresenius, J. Anal. Chem.* **2001**, *369*, 320–327.

(17) Mao, X.; Zeng, X.; Wen, S.-B.; Russo, R. E. *Spectrochim. Acta, Part B* **2005**, *60*, 960–967.

(18) Cristoforetti, G.; Legnaioli, S.; Palleschi, V.; Salvetti, A.; Tognoni, E. *Spectrochim. Acta, Part B* **2004**, *59*, 1907–1917.

(19) Michel, A. P. M.; Lawrence-Snyder, M.; Angel, S. M.; Chave, A. D. *Appl. Opt.* **2007**, *46*, 2507–2515.

(20) Pardede, M.; Kurniawan, H.; Tjia, M. O.; Ikezawa, K.; Maruyama, T.; Kagawa, K. *Appl. Spectrosc.* **2001**, *55*, 1229–1236.

(21) Scaffidi, J.; Pearman, W.; Carter, J. C.; Colston, B. W., Jr; Angel, S. M. *Appl. Opt.* **2004**, *43*, 6492–6499.

(22) Stepputat, M.; Noll, R. *Appl. Opt.* **2003**, *42*, 6210–6220.

(23) Gautier, C.; Fichet, P.; Menut, D.; Lacourt, J.-L.; L'Hermite, D.; Dubessy, J. *Spectrochim. Acta Part B* **2005**, *60*, 792–804.

(24) Rai, V. N.; Yueh, F.-Y.; Singh, J. P. *Appl. Opt.* **2003**, *42*, 2094–2101.

(25) Rehse, S. J.; Ryder, C. A. *Spectrochim. Acta, Part B* **2009**, *64*, 974–980.

(26) Colao, F.; Lazic, V.; Fantoni, R.; Pershin, S. *Spectrochim. Acta, Part B* **2002**, *57*, 1167–1179.

(27) Rai, V. N.; Yueh, F. Y.; Singh, J. P. *Appl. Opt.* **2008**, *47*, G21–G29.

(28) Corsi, M.; Cristoforetti, G.; Giuffrida, M.; Hidalgo, M.; Legnaioli, S.; Palleschi, V.; Salvetti, A.; Tognoni, E.; Vallebona, C. *Spectrochim. Acta, Part B* **2004**, *59*, 723–735.

(29) Hasegawa, T.; Haraguchi, H. In *Inductively Coupled Plasmas in Analytical Atomic Spectrometry*; Montaser, A.; Golightly, D. W., Ed.; VCH: New York, 1987.

(30) Chan, S.; Montaser, A. *Spectrochim. Acta* **1989**, *44B*, 175–184.

(31) Griem, H. R. *Spectral Line Broadening by Plasmas*; Academic Press: New York, 1974.

(32) Weise, W. L. In *Plasma Diagnostic Techniques*; Huddlestone, R. H.; Leonard, S. L.,, Ed.; Academic Press: New York, 1965.

(33) Griem, H. R. *Principles of Plasma Spectroscopy*; Cambridge University Press: New York, 1997.

(34) Yalçin, Ş.; Crosley, D. R.; Smith, G. P.; Faris, G. W. *Appl. Phys. B: Laser Opt.* **1999**, *68*, 121–130.

(35) Kumar, A.; Yueh, F. Y.; Singh, J. P. *Appl. Opt.* **2003**, *42*, 6047–6051.